Received 6 October 2020; revised 19 November 2020; accepted 22 November 2020. Date of publication 26 November 2020; date of current version 28 January 2021. The review of this article was arranged by Editor A. Nathan.

Digital Object Identifier 10.1109/JEDS.2020.3040771

Pixellated Perovskite Photodiode on IGZO Thin Film Transistor Backplane for Low Dose Indirect X-Ray Detection

TAOYU ZOU[1,2], BEN XIANG[1], YANGBING XU[3], YA WANG[1], CHUAN LIU[3] (Member, IEEE), JUN CHEN[3] (Member, IEEE), KAI WANG[3] (Member, IEEE), QING DAI[4], SHENGDONG ZHANG[1] (Senior Member, IEEE), YONG-YOUNG NOH[2] (Member, IEEE), AND HANG ZHOU[1] (Member, IEEE)

1 School of Electronic and Computer Engineering, Peking University Shenzhen Graduate School, Shenzhen 518055, China
2 Department of Chemical Engineering, Pohang University of Science and Technology (POSTECH), Pohang 37673, South Korea
3 State Key Laboratory of Optoelectronic Materials and Technologies, School of Electronics and Information Technology, Sun Yat-sen University, Guangzhou 510006, China
4 Division of Nanophotonics, CAS Center for Excellence in Nanoscience, National Center for Nanoscience and Technology, Beijing 100190, China

CORRESPONDING AUTHORS: C. LIU; Y. NOH; and H. ZHOU (e-mail: liuchuan5@mail.sysu.edu.cn; yynoh@postech.ac.kr; zhouh81@pkusz.edu.cn)

This work was supported in part by the National Key Research and Development Program of China under Grant 2016YFA0202002; in part by the Shenzhen Municipal Scientific Program under Grant JCYJ20200109140610435; in part by the National Natural Science Foundation of China under Grant 61974006; and in part by the Guangdong Natural Science Foundation under Grant 2018A030313332. The work of Chuan Liu was supported by the Guangdong Provincial Department of Science and Technology under Grant 2019B010924002. The work of Yong-Young Noh was supported by the Center for Advanced Soft-Electronics funded by National Research Foundation of Korea through the Ministry of Science and ICT under Grant 2013M3A6A5073183 and Grant 2014M3A6A5060932.This paper has supplementary downloadable material available at https://ieeexplore.ieee.org, provided by the authors.

ABSTRACT The integration of perovskite photodetectors with thin-film transistor (TFT) backplane or complementary metal-oxide-semiconductor CMOS circuit is a key step towards prototyping perovskite-based image sensors. Here, we demonstrate a pixel configuration for indirect X-ray detection comprising of IGZO TFTs and perovskite photodiodes (PDs). The perovskite photodiode is patterned by a two-step deposition method. Our integrated TFT/PD pixel shows a weak light detection capability down to 4 nW cm^{-2}, and a fast-transient response to the pulse light and gate switching. Combining with a CsI scintillator, the integrated pixel achieves a specific X-ray sensitivity of 8.2 $\times$ $10^2 \mu C$ mGy_{air}^{-1} cm^{-3}. Theoretically, with a state-of-the-art scintillator, the new pixel can provide a detectable signal for X-ray imaging at a dose rate as low as 10 μGy_{air} s^{-1}. This work provides an advanced pixel design for high resolution, high sensitivity, and high frame-rate flat-panel imager.

INDEX TERMS Flat-panel imager, IGZO, perovskite, thin-film transistors, X-ray detectors.

I. INTRODUCTION

Flat panel image sensors have wide applications in biomedical imaging and industrial inspection. These image sensors are usually cataloged into two types: passive pixel and active pixel, both of which require integration of photodiode (PD) with thin-film transistors. The modern X-ray radiography requires a more advanced imaging panel that provides higher resolution and sensitivity for low dose detection. It is therefore imperative to develop a new generation image sensor for X-ray detection using the latest technologies. To achieve a low cost and high-performance system, factors like material selection, device architecture, and processing compatibility have to be well optimized.

Perovskite-based materials are considered as promising materials for optoelectronic devices covering a wide range of wavelengths from near-infrared to a high energy photon especially in ionizing radiation detection, such as X-ray and γ-ray detection [1]. Due to the large light absorption coefficient and defect-tolerant nature of perovskite thin films, perovskite photodiodes show excellent figures-of-merits, such as high responsivity and detectivity. However, when compared with their silicon counterpart, more efforts are needed

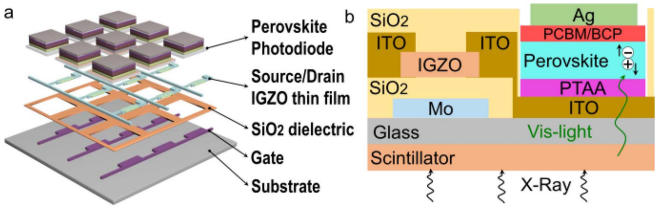

FIGURE 1. (a) Layer structures of the integrated IGZO TFT/perovskite photodiode pixel array, (b) Schematic view of the integrated IGZO TFT/perovskite photodiode pixel array with a scintillator for indirect X-ray detection.

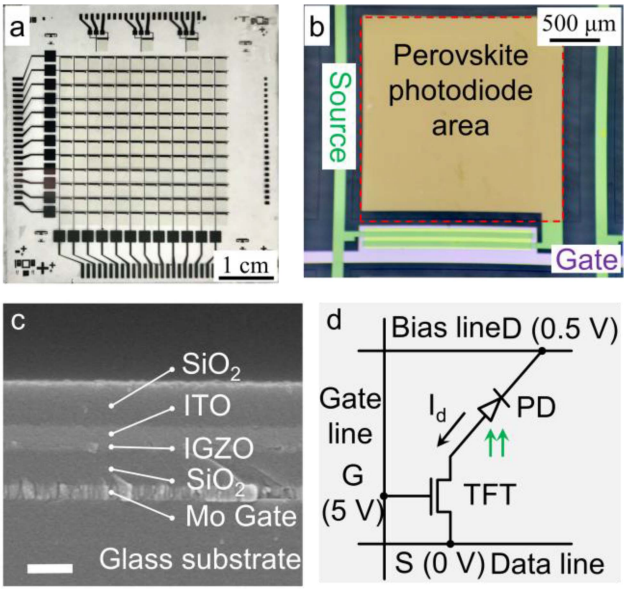

FIGURE 2. (a) The as-prepared 12 × 12 IGZO TFT array, the size of the glass substrate is 5 cm × 5 cm. (b) Optical microscope image of a single IGZO TFT pixel, respectively. The length and width of the IZGO TFT are 40 μm and 1600 μm. The dimension of the perovskite photodiode area is 2 mm × 2 mm. (c) The cross-sectional SEM image of the IGZO TFT. The scale bar is 250 nm. (d) The equivalent circuit diagram of the TFT/PD pixel.

to achieve a lower dark current and higher stability in perovskite PDs [2]. The dark current level of the best amorphous silicon diode is in the fA range for a 148×148 μm^2 pixel [2]. Imaging pixel that comprises perovskite photodiode and TFT should have the potential to bring a disruptive change on the indirect X-ray imaging. Nonetheless, reports on the integration of IGZO TFT and perovskite photodiode for X-ray detections are limited. Our previous study reveals that MA^+ may cause a malfunction of the underneath IGZO TFT [3]. On the other hand, the work by Zakhidov group demonstrated that patterned perovskite thin film may help to minimize the cross-talk between neighboring pixels [4]. It also remains an open question whether the integrated pixel of perovskite photodiode and IGZO TFT is suitable for direct or indirect X-ray imaging, or both.

Here, in an attempt of combining the merits of perovskite photodiode and IGZO TFT, we have fabricated pixel arrays formed by perovskite photodiodes and IGZO-TFTs. The device performance of the integrated X-ray detector under indirect detection mode is investigated.

II. DEVICE ARCHITECTURE AND FABRICATION

The integrated IGZO TFT/perovskite PD for X-ray detection was fabricated on a 5 cm × 5 cm glass substrate with the device structure shown in Fig. 1. The IGZO TFTs, with bottom gate and top contact structure, were fabricated by conventional sputtering and photolithography processes. First, an 80 nm thick Mo was radio frequency sputtered and patterned as the gate electrode, SiO_2 (200 nm) was then deposited by PECVD. A 40 nm thick IGZO was RF-sputtered at room temperature and patterned via lift-off technique. Next, an 80 nm ITO was RF-sputtered as the source and drain electrodes. Finally, another SiO_2 layer was deposited as an encapsulation layer which protected the IGZO thin film from potential damages in the subsequent perovskite fabricating process [3]. The as-fabricated 12 × 12 IGZO TFT array is shown in Figure 2a, with the top view of a single IGZO TFT with ITO drain pad for perovskite photodiode area are shown in Fig. 2b. The width/length of the IGZO TFT is 1600 μm/40 μm. The cross-sectional SEM image of the drain electrode region of the IGZO TFT is shown in Fig. 2c. Fig. 2d shows the equivalent circuit diagram of the TFT/PD pixel. In total, 6 masks are used in our work. 4 photomasks are used for the fabrication of IGZO TFT and 2 fine-metal masks are for the perovskite photodiode fabrication. For comparison, 12 masks are required for typical conventional optical sensor fabrication [5], [6].

For image sensor applications, ideally, the photodiode should have high responsivity and detectivity, and low dark current. Our previous studies reveal the performance of perovskite photodiode, particularly the dark current, is strongly affected by its device structure and interlayer [7]–[10]. Interface engineering is one of the effective strategies to reduce leakage currents in perovskite photodiodes. In this work, poly (bis(4-phenyl) (2 ,4, 6-trimethylphenyl)amine (PTAA) is chosen as the hole transporting layer for a low dark current of perovskite photodiode. It is reported that the HOMO level of the PTAA matches the valence band of perovskite thin film and plays an important role in increasing the grain size and decreasing the grain boundary of perovskite [11].

In this work, PTAA (Wuhan LinkZill Technology Co., Ltd.) was dissolved in 1,2-dichlorobenzene with a concentration of 2 mg/ml and was spin-coated on the as-prepared TFT array in Fig. 2a. We adopted a two-step thermal evaporation method to realize the patterning of perovskite thin films. Briefly, a layer of PbI_2 (150 nm) was thermally evaporated on the top of the PTAA layer using a fine-metal mask. Next, methylammonium iodide (MAI) solution (30 mg/ml) was spin-coated on the patterned PbI_2 thin film. The stack films were then annealed at 100 °C to form patterned perovskite thin film. The unreacted MAI was washed by isopropanol solution. Subsequently, $PC_{61}BM$ and BCP were spin-coated at 2000 rpm for 60 s and annealed at 100 °C for 10 min.

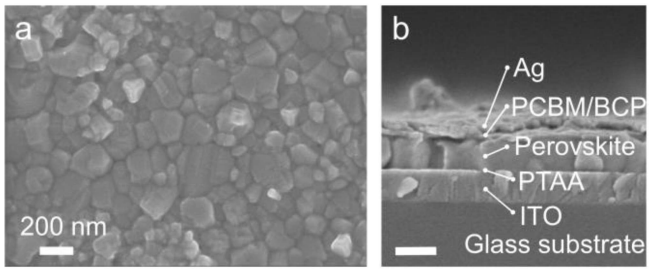

FIGURE 3. (a) SEM image of as-prepared perovskite thin-film via two-step method fabrication. (b) The cross-sectional SEM image of the perovskite photodiode. The scale bar is 250 nm.

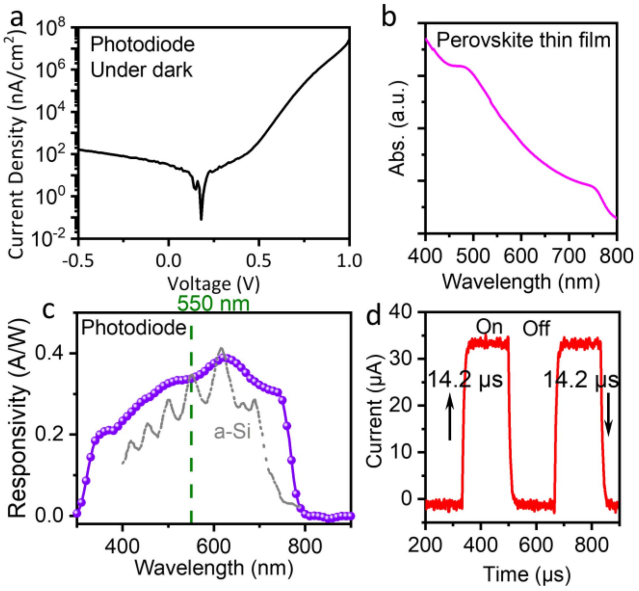

FIGURE 4. (a) I-V curve of an inverted perovskite photodiode measured under dark. (b) The absorption spectrum of perovskite thin film. (c) Responsivity (R) of the perovskite photodiode (solid line) and a conventional a-Si photodiode (dotted-line) calculated from their external quantum efficiency. (d) The transient response of a perovskite photodiode under the illumination of 550 nm green light.

Finally, patterned Ag electrodes were thermally evaporated under high vacuum ($\sim 5\times10^{-4}$ Pa) with a shadow mask. The area of the thermal-evaporated top Ag electrode with a shadow mask is about 0.28 mm^2, which defines the active area of the perovskite photodiode. The perovskite thin-film deposition area is 2 mm × 2 mm as shown in Fig. 2b. Thus, the maximum fill factor could be up to ~60%, depending on the area of the top electrode. The surface morphology of the as-prepared perovskite thin film is shown in Fig. 3a. A densely packed morphology with large grain boundaries is observed in our perovskite thin film, with an average grain size of ~200 nm. Fig. 3b shows the cross-section SEM images of the perovskite photodiode. The thickness of the perovskite thin film is about 230 nm.

III. RESULT AND DISCUSSION

In the integrated TFT/PD pixel, the dark current level (or more precisely the noise equivalent power) of the perovskite photodiode will determine the weak light detection capability [12]. As shown in Fig. 4a, with a diode structure of ITO/PTAA/Perovskite/PCBM/BCP/Ag, the dark current of a perovskite photodiode is ~47 nA/cm^2 and ~163 nA/cm^2 when biased at −0.1 V and −0.5 V, respectively. Our previous work shows a good uniformity of 10 × 10 photodiode arrays fabricated using the same fabrication method [9], [13], in which the median dark current value is 115 nA/cm^2 and the median photocurrent value is 9.73±2.39 mA/cm^2. So far, the dark current level of the best-reported perovskite photodiodes was ~14 nA/cm^2 at −0.3 V [11], [14], where weak light detection in the sub-picowatt per square centimeter range is achieved. The UV-vis absorption spectrum of the perovskite film (Fig. 4b) indicates a broad light absorption at the visible region up to 800 nm. The calculated responsivity for perovskite photodiode is ~0.34 A/W at 550 nm, which is close to the a-Si:H photodiode (0.35 A W^{-1}) [15], as shown in Fig. 4c. In Fig. 4d, the perovskite photodiode shows a short rise and fall time of ~14.2 µs under the illumination of pulse switching green light LED, while the fluorescence decay time of the commercial CsI:Tl scintillators is ~1 µs [16], [17]. The response speed of a photodiode is mainly determined by the charge transport and collection, which is influenced by, for example, the charge mobility, the interfacial charge transport materials, trap states at the interface, the thickness of the device, and applied electrical bias [18]–[21].

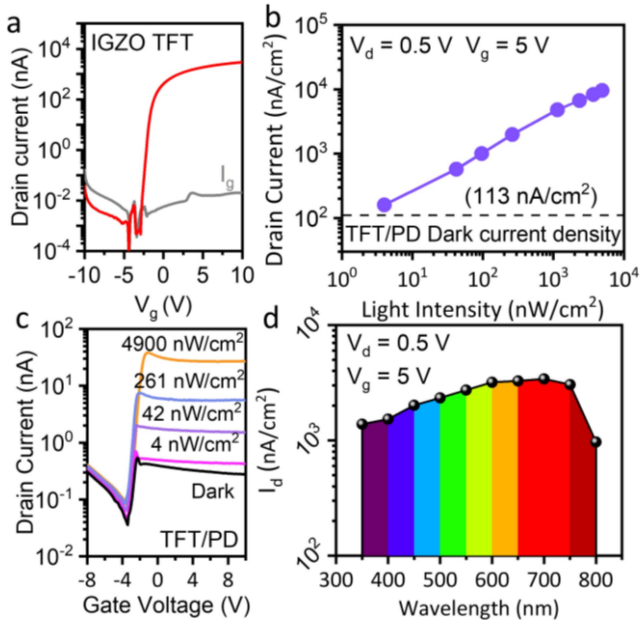

FIGURE 5. (a) Transfer characteristics of a typical IGZO TFT at V_d = 0.1 V and corresponding I_g curve. (b) Photocurrent density of a TFT/PD pixel at Vg = 5 V and Vd = 0.5 V as a function of incident light intensity. (c) Transfer characteristics of a pixelated TFT connected with a perovskite PD under various light intensities. (d) Photocurrent of a pixel at V_g = 5 V and V_d = 0.5 V as a function of light wavelength (light intensity is 1 µW/cm^2).

The transfer characteristics of a typical IGZO TFT fabricated in this work are shown in Fig. 5a with drain-to-source

voltage $V_d = 0.1$ V. The calculated carrier mobility of our IGZO TFT is 7.5 $cm^2/(V{\cdot}s)$, which is beneficial for designing high-density pixels arrays for high-resolution imaging panel. The transfer characteristics of a typical IGZO TFT (W/L = 1600 μm/40 μm) show an off-state drain current $\sim 10^{-11}$ A at gate biased at −4V, which is comparable to the a-Si:H TFT in a commercial flat panel imager [22]. Fig. 5b shows the photoresponse of the integrated TFT/PD pixel measured under 520 nm light with intensity varied from 0 to 4.9 μW/cm^2. When the TFT was switched on ($V_g > -2$ V) (Fig. 5c), the on-state dark current is apparently limited by the dark current of the perovskite photodiode, which is ∼ 0.32 nA, corresponding to a dark current intensity of ∼113 nA/cm^2 of the perovskite photodiode. Under illumination, the integrated pixel shows significant photoresponse to 550 nm light with measurable intensity down to 4 nW/cm^2. The increased off current after integrating perovskite photodiode in Fig. 5c compared with that before integration in Fig. 5a can be contributed to the fabrication process of perovskite thin film, particularly the MA^+, as revealed in our previous study that MAI could increase the off-current of IGZO TFT [3].

Furthermore, the photoresponse current density of the integrated TFT/PD pixel to different light wavelength is investigated by fixing the incident light intensity at 1 μW cm^{-2}, as shown in Fig. 5d, manifesting that our integrated photodetector is capable of detecting the completely visible region from 400 nm to 750 nm. Therefore, the perovskite PD integrated pixel can be adapted to many different types of scintillators in the X-ray detection system.

For indirect X-ray detection, the photocurrent of the perovskite photodiode is mainly determined by the conversion efficiency (light output) of the scintillator and the EQE of the perovskite photodiode. A CsI-Tl scintillator was used in our work with the radioluminescence peak at 547 nm (Fig. 6a). The X-ray source is from VJ Technologies China (Suzhou) Co., Ltd. (MODEL: IXS080BP210P396), with a maximum power output of 210 W. The radiation dose rate of the incident X-ray can be modulated by controlling the output voltage from 20 kV to 80 kV, and was carefully calibrated by using a standard dosimeter. Fig. 6c shows the photocurrent of a single perovskite PD in ambient air without encapsulation, under various X-ray dose rate, with a measurable photocurrent of ∼2.5 nA at a dose rate as low as 2.0 mGy_{air}/s. The calculated specific sensitivity for the perovskite photodiode under the indirect X-ray detection is $\sim 7.2 \times 10^2$ $\mu C{\cdot}mGy_{air}^{-1}{\cdot}cm^{-3}$) (or 16.5 $\mu C{\cdot}Gy_{air}^{-1}{\cdot}cm^{-2}$)) at an X-ray dose of 2 mGy_{air}/s. The value is comparable to previous X-ray detectors based on perovskite single crystals, [23]–[25] and is 3 times higher than that of α-Se detectors under direct detection [26]. The sensitivity is still lower than that of some perovskite-based direct X-ray detector, such as single crystal perovskite, [27]–[31] quantum dots, [32] perovskite wafer, [33] 2D hybrid perovskite, [34] and polycrystalline perovskite, [35] which shows a sensitivity of $\sim 10^3$ to 10^4 $\mu C\ Gy_{air}^{-1}{\cdot}cm^2$). The state-of-the-art a-Si:H based indirect

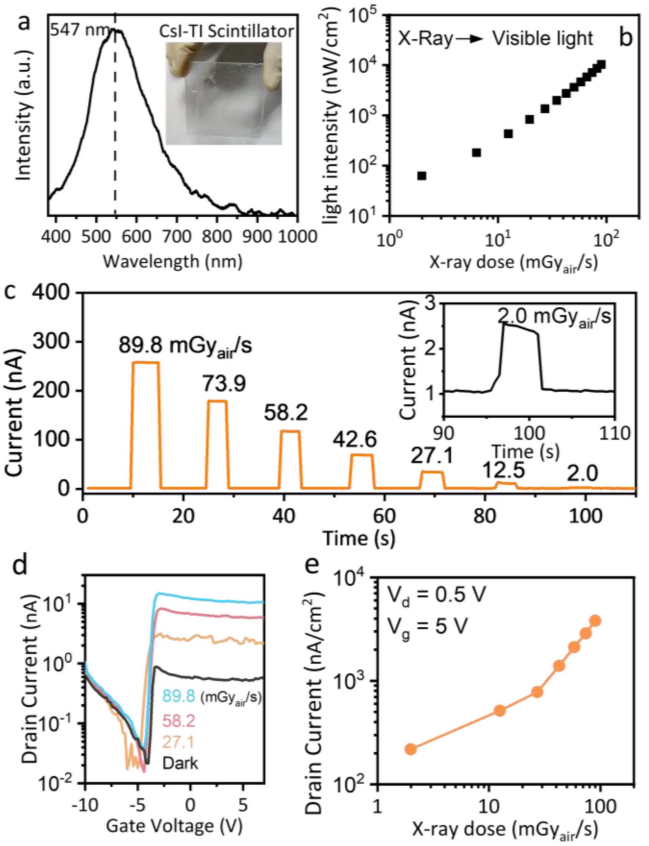

FIGURE 6. (a) Luminescence spectrum of a CsI-Tl scintillator under X-ray illumination. The inset is the image of the CsI-Tl scintillator used in our work. (b) Radioluminescence intensity (Light output) of the CsI-Tl scintillator as a function of the X-ray dose rate. (c) Response of a perovskite photodiode (size: 0.04 cm^2) under indirect detection mode with CsI:Tl scintillator upon exposure to X-ray with dose rates decreasing from 89.8 mGy_{air}/s to 2 mGy_{air}/s over time. The device was measured in ambient air without encapsulation. (The ambient temperature and humidity of the measuring environment was 25°C and ∼50%, respectively). (d) semi-log plots of the transfer characteristics of a TFT/PD pixel exposed to various X-Ray dose rate (V_d = 0.5 V). (e) Photocurrent response of the IGZO TFT/perovskite photodiode pixel at Vg = 5 V and Vd = 0.5 V as a function of incident X-Ray dose rate in an indirect detection mode.

x-ray detector can be used well below 10 nGy_{air}, in which the detective quantum efficiency (DQE) is above 45% at 5 nGy_{air} and 1 lp/mm [2].

The sensitivity of the perovskite PD under X-ray exposure is significantly limited by the scintillator in our experiment. The performance of the CsI:Tl scintillator adopted in this work falls behind the state-of-the-art scintillator due to a poor storage environment. The output light intensity of the CsI:Tl scintillator used in this work varies from 62 nW/cm^2 to 1.0×10^4 nW/cm^2 in the X-ray dose rate range from 2 mGy_{air}/s to 89.8 mGy_{air}/s (Fig. 6b), which is lower than that of GOS scintillator reported by Heo *et al.* [36] in which the output light intensity is ∼12 μW/cm^2 in an X-ray dose rate of 100 $\mu Gy_{air}/s$. For comparison, a high-quality scintillator for a low dose X-ray detection system can provide a light intensity of 15 nW/cm^2 at a dose rate of 10 $\mu Gy_{air}/s$ [37], which is within the detection limit of our integrated pixel (4 nW/cm^2 as shown in Fig. 5b). Therefore, if

a scintillator with higher light yield was adopted in this work, such as Rb_2CuBr_3 scintillator [38] and CsPbBr3 perovskite nanocrystals scintillator, [36] low dose X-ray detection could be expected.

We then exposed the integrated pixel to various X-ray radiation dose rates ranging from 89.8 mGy_{air}/s to 2 mGy_{air}/s to measure its detection performance. As shown in Figs. 6d and e, the on-state drain current of the integrated pixel increases with the incident X-ray radiation dose rate. The measured response current (I_d) is 218 nA/cm^2 which converts to a specific sensitivity of 8.2×10^2 $\mu C \cdot mGy_{air}^{-1} \cdot cm^{-3}$ or 16.4 $\mu C \cdot Gy_{air}^{-1} \cdot cm^{-2}$ to a dose rate of 2 mGy_{air}/s. The CsI:Tl scintillator has effectively absorbed most of the X-ray and protect the integrated pixel from direct X-ray exposure. It has been reported previously that IGZO TFT would suffer from increased gate leakage current (I_g) when subject to direct X-ray exposure due to the trapping of hole charges in the dielectric layer [39]. Fig. S1a shows that the IGZO TFT maintains a relatively low gate leakage current during X-ray exposure with CsI:Tl scintillator compared with that of IGZO TFT under direct exposure without CsI:Tl scintillator (Fig. S1b).

IV. CONCLUSION

In summary, the perovskite photodiode, which is patterned by a two-step deposition method, presents a low dark current of ~47 nA/cm^2 at −0.1 V. Our integrated TFT/PD pixel shows a weak light detection capability down to 4 nW/cm^2. Combining with a CsI-Tl scintillator, the integrated IGZO TFT/Perovskite PD pixel shows a specific sensitivity of 8.2×10^2 $\mu C/(mGy_{air} \cdot cm^3)$, The integrated photodetector shows a high photoresponse to a broad spectrum covering 350-800 nm, indicating its compatibility with different scintillators. The pixel configuration described in this work is very promising for future low dose X-ray detection applications.

REFERENCES

[1] H. Wei and J. Huang, "Halide lead perovskites for ionizing radiation detection," *Nat. Commun.*, vol. 10, no. 1, p. 1066, Mar. 2019, doi: 10.1038/s41467-019-08981-w.

[2] T. Ducourant *et al.*, "Latest advancements in state-of-the-art aSi-based x-ray flat panel detectors," in *Proc. SPIE Med. Imag.*, 2018, Art. no. 105735V.

[3] X. Xu *et al.*, "Enhanced detectivity and suppressed dark current of Perovskite–InGaZnO phototransistor via a PCBM interlayer," *ACS Appl. Mater. Interfaces*, vol. 10, no. 50, pp. 44144–44151, 2018, doi: 10.1021/acsami.8b16346.

[4] D. Lyashenko, A. Perez, and A. Zakhidov, "High-resolution patterning of organohalide lead perovskite pixels for photodetectors using orthogonal photolithography," *Phys. Status Solidi A*, vol. 214, no. 1, 2017, Art. no. 1600302, doi: 10.1002/pssa.201600302.

[5] X. Zhou *et al.*, "Vertically integrated optical sensor with photoconductive gain > 10 and fill factor > 70%," *IEEE Electron Device Lett.*, vol. 39, no. 3, pp. 386–389, Mar. 2018, doi: 10.1109/led.2018.2792003.

[6] X. Zhou *et al.*, "39–2: Highly sensitive a-Si:H PIN photodiode gated LTPS TFT for optical in-display fingerprint identification," *SID Symp. Dig. Tech. Papers*, vol. 49, no. 1, pp. 490–493, 2018, doi: 10.1002/sdtp.12608.

[7] D. Luo *et al.*, "Low-dimensional contact layers for enhanced perovskite photodiodes," *Adv. Funct. Mater.*, vol. 30, no. 24, 2020, Art. no. 2001692, doi: 10.1002/adfm.202001692.

[8] T. Zou *et al.*, "Reduced graphene oxide-induced crystallization of CuPc interfacial layer for high performance of perovskite photodetectors," *RSC Adv.*, vol. 9, no. 7, pp. 3800–3808, 2019, doi: 10.1039/c8ra08864k.

[9] T. Zou *et al.*, "Enhanced UV-C detection of perovskite photodetector arrays via inorganic CsPbBr3 quantum dot down-conversion layer," *Adv. Opt. Mater.*, vol. 7, no. 11, 2019, Art. no. 1801812, doi: 10.1002/adom.201801812.

[10] W. Luo *et al.*, "High detectivity ITO/organolead halide perovskite Schottky photodiodes," *Semicond. Sci. Technol.*, vol. 34, no. 7, 2019, Art. no. 074004, doi: 10.1088/1361-6641/ab075d.

[11] L. Shen *et al.*, "A self-powered, sub-nanosecond-response solution-processed hybrid perovskite photodetector for time-resolved photoluminescence-lifetime detection," *Adv. Mater.*, vol. 28, no. 48, pp. 10794–10800, 2016, doi: 10.1002/adma.201603573.

[12] T. Takahashi *et al.*, "Carbon nanotube active-matrix backplanes for mechanically flexible visible light and X-ray imagers," *Nano Lett.*, vol. 13, no. 11, pp. 5425–30, 2013, doi: 10.1021/nl403001r.

[13] T. Zou *et al.*, "Flexible, active-matrix flat-panel image sensor for low dose X-ray detection enabled by integration of perovskite photodiode and oxide thin film transistor," in *Proc. IEEE Int. Electron Devices Meet. (IEDM)*, Dec. 2019, pp. 8. 5.1–8.5.4, doi: 10.1109/IEDM19573.2019.8993639.

[14] Y. Fang and J. Huang, "Resolving weak light of sub-picowatt per square centimeter by hybrid perovskite photodetectors enabled by noise reduction," *Adv. Mater.*, vol. 27, no. 17, pp. 2804–2810, 2015, doi: 10.1002/adma.201500099.

[15] R. L. Weisfield, "Large-area amorphous silicon TFT-based X-ray image sensors for medical imaging and non destructive testing," in *Proc. 4th Symp. Thin Film Transistor Technol. Electrochem. Soc.*, vol. 98, no. 22, 1999, pp. 369–380.

[16] S. Jagtap, P. Chopade, S. Tadepalli, A. Bhalerao, and S. Gosavi, "A review on the progress of ZnSe as inorganic scintillator," *Opto-Electron. Rev.*, vol. 27, no. 1, pp. 90–103, 2019, doi: 10.1016/j.opelre.2019.01.001.

[17] F. Cao *et al.*, "Shining emitter in a stable host: Design of halide perovskite scintillators for X-ray imaging from commercial concept," *ACS Nano*, vol. 14, no. 5, pp. 5183–5193, May 2020, doi: 10.1021/acsnano.9b06114.

[18] L. Dou *et al.*, "Solution-processed hybrid perovskite photodetectors with high detectivity," *Nat. Commun.*, vol. 5, p. 5404, Nov. 2014, doi: 10.1038/ncomms6404.

[19] R. D. J.-V. Vuuren, A. Armin, A. K. Pandey, P. L. Burn, and P. Meredith, "Organic photodiodes: The future of full color detection and image sensing," *Adv. Mater.*, vol. 28, no. 24, pp. 4766–802, Jun. 2016, doi: 10.1002/adma.201505405.

[20] T. Zhang *et al.*, "High speed and stable solution-processed triple cation perovskite photodetectors," *Adv. Opt. Mater.*, vol. 6, no. 13, 2018, Art. no. 1701341, doi: 10.1002/adom.201701341.

[21] J. Zhou and J. Huang, "Photodetectors based on organic-inorganic hybrid lead halide perovskites," *Adv. Sci.*, vol. 5, no. 1, 2018, Art. no. 1700256, doi: 10.1002/advs.201700256.

[22] H. Lee, G. Yoo, J.-S. Yoo, and J. Kanicki, "Asymmetric electrical properties of fork a-Si: H thin-film transistor and its application to flat panel displays," *J. Appl. Phys.*, vol. 105, no. 12, 2009, Art. no. 124522, doi: 10.1063/1.3153968.

[23] H. Wei *et al.*, "Sensitive X-ray detectors made of methylammonium lead tribromide perovskite single crystals," *Nat. Photon.*, vol. 10, no. 5, pp. 333–339, 2016, doi: 10.1038/nphoton.2016.41.

[24] F. Yao *et al.*, "Room-temperature liquid diffused separation induced crystallization for high-quality perovskite single crystals," *Nat. Commun.*, vol. 11, no. 1, p. 1194, Mar. 2020, doi: 10.1038/s41467-020-15037-x.

[25] W. Pan *et al.*, "$Cs_2AgBiBr_6$ single-crystal X-ray detectors with a low detection limit," *Nat. Photon.*, vol. 11, pp. 726–732, Nov. 2017, doi: 10.1038/s41566-017-0012-4.

[26] S. O. Kasap, "X-ray sensitivity of photoconductors: Application to stabilized a-Se," *J. Phys. D, Appl. Phys.*, vol. 33, no. 21, pp. 2853–2865, 2000, doi: 10.1088/0022-3727/33/21/326.

[27] R. Zhuang *et al.*, "Highly sensitive X-ray detector made of layered perovskite-like $(NH_4)_3Bi_2I_9$ single crystal with anisotropic

response," *Nat. Photon.*, vol. 13, no. 9, pp. 602–608, 2019, doi: 10.1038/s41566-019-0466-7.
[28] W. Wei *et al.*, "Monolithic integration of hybrid perovskite single crystals with heterogenous substrate for highly sensitive X-ray imaging," *Nat. Photon.*, vol. 11, no. 5, pp. 315–321, 2017, doi: 10.1038/nphoton.2017.43.
[29] Y. Huang et al., "A-site cation engineering for highly efficient $MAPbI_3$ single-crystal X-ray detector," *Angew. Chem. Int. Ed. Engl.*, vol. 58, no. 49, pp. 17834–17842, Dec. 2019, doi: 10.1002/anie.201911281.
[30] X. Wang *et al.*, "Ultrafast ionizing radiation detection by p-n junctions made with single crystals of solution-processed perovskite," *Adv. Electron. Mater.*, vol. 4, no. 11, Nov. 2018, Art. no. 1800237, doi: 10.1002/aelm.201800237.
[31] X. Zheng *et al.*, "Ultrasensitive and stable X-ray detection using zero-dimensional lead-free perovskites," Journal of Energy Chemistry, vol. 49, pp. 299–306, Oct. 2020, doi: 10.1016/j.jechem.2020.02.049.
[32] J. Liu *et al.*, "Flexible, printable soft-X-ray detectors based on all-inorganic perovskite quantum dots," *Adv. Mater.*, vol. 31, no. 30, Jul. 2019, Art. no. e1901644, doi: 10.1002/adma.201901644.
[33] S. Shrestha *et al.*, "High-performance direct conversion X-ray detectors based on sintered hybrid lead triiodide perovskite wafers," vol. 11, pp. 436–440, Jun. 2017, doi: 10.1038/nphoton.2017.94.
[34] C. Ji *et al.*, "2D hybrid perovskite ferroelectric enables highly sensitive X-ray detection with low driving voltage," *Adv. Funct. Mater.*, vol. 30, no. 5, 2020, Art. no. 1905529, doi: 10.1002/adfm.201905529.
[35] Y. C. Kim *et al.*, "Printable organometallic perovskite enables large-area, low-dose X-ray imaging," *Nature*, vol. 550, no. 7674, pp. 87–91, Oct. 2017, doi: 10.1038/nature24032.
[36] J. H. Heo, D. H. Shin, J. K. Park, D. H. Kim, S. J. Lee, and S. H. Im, "High-performance next-generation perovskite nanocrystal scintillator for nondestructive X-ray imaging," *Adv. Mater.*, vol. 30, Aug. 2018, Art. no. e1801743, doi: 10.1002/adma.201801743.
[37] G. H. Gelinck *et al.*, "X-ray detector-on-plastic with high sensitivity using low cost, solution-processed organic photodiodes," *IEEE Trans. Electron Devices*, vol. 63, no. 1, pp. 197–204, Jan. 2016, doi: 10.1109/TED.2015.2432572.
[38] B. Yang *et al.*, "Lead-free halide Rb_2CuBr_3 as sensitive X-ray scintillator," *Adv. Mater.*, vol. 31, no. 44, Nov. 2019, Art. no. e1904711, doi: 10.1002/adma.201904711.
[39] T. Cramer *et al.*, "Radiation-tolerant flexible large-area electronics based on oxide semiconductors," *Adv. Electron. Mater.*, vol. 2, no. 7, 2016, Art. no. 1500489, doi: 10.1002/aelm.201500489.